Microstructure-dependent predictions of the effect of defect size and shape on the high-cycle fatigue strength

Raphaël Guerchais, Franck Morel, Nicolas Saintier

Microstructure-dependent predictions of the effect of defect size and shape on the high-cycle fatigue strength

R. Guerchais[1], F. Morel[2] and N. Saintier[3]

[1] Arts et Metiers ParisTech, LAMPA, 2 bd du Ronceray, 49035 Angers Cedex, France, raphael.guerchais@ensam.eu
[2] franck.morel@ensam.eu
[3] Arts et Metiers ParisTech, I2M – UMR CNRS 5295, Esplanade des Arts et Métiers, 33405 Talence Cedex, France, nicolas.saintier@ensam.eu

ABSTRACT. *This study aims to investigate the effects of both the microstructure and void on the high-cycle fatigue behavior of metallic materials. To deal with this matter, finite element analyses of polycrystalline aggregates are carried out, for different configurations of crystalline orientations, in order to estimate the mechanical state, at the grain scale, in the vicinity of a small elliptical hole. Fatigue criteria are then applied to predict the average fatigue limit in fully reversed tension, for different defect sizes and ellipse aspect ratios. The constitutive models and the fatigue criteria are calibrated using experimental data obtained from specimens made of 316L austenitic steel. The predictions are then confronted to experimental trends.*

INTRODUCTION

The high-cycle fatigue strength of metallic material, in addition to being strongly influenced by the microstructure, may be significantly affected by the presence of defects and it is thus important to be able to quantify their detrimental effect. Murakami and Endo have shown that the defect size $\sqrt{area}$, expressed by the square root of the area of the defect projected in the direction of the maximum principal stress, is a crucial parameter to determine the fatigue strength [1]. The authors even considered $\sqrt{area}$ as a sufficient geometrical parameter to estimate the fatigue limit. However, Billaudeau et al. have shown from fatigue tests carried out on specimens made of low carbon steel (C36) and containing an artificial notch that the fatigue limit is affected not only by the size of the defect $\sqrt{area}$ but also by its morphology [2]. More precisely, the authors have highlight that, for a given defect size $\sqrt{area}$, an increase in the stress concentration factor K_t:

- induces a significant decrease in the fatigue strength in the case where $K_t \in [1;2]$,
- leads to a slight increase in the fatigue limit in the case where $K_t \in [2;4]$.

The objective is to analyze this issue from a numerical point of view, in the continuation of previous works [3,4]. More precisely, finite element analyses of two-dimensional polycrystalline aggregates, loaded in fully reversed tension, are conducted in order to estimate the mechanical state, at the grain scale, in microstructures containing a small elliptical hole. Two fatigue criteria are then calibrated thanks to the results of the FEA and experimental data obtained from fatigue tests conducted on specimens, made of 316L austenitic steel, with and without a hemispherical notch [3]. The predictions of these criteria are then determined for different defect sizes and ellipse aspect ratios and are compared to the experimental trends.

POLYCRYSTALLINE AGGREGATE MODEL

Finite element model of the polycrystalline aggregates

The geometry of the polycrystal is defined by a partition of a two-dimensional square-shaped domain into convex polygonal subdomains obtained with a Voronoi decomposition. Due to the dimension chosen for the polycrystal (see Fig. 1), 3265 seeds are used in the Voronoi tessellation so that the mean grain size in the numerical model corresponds to the mean grain size of the material tested [3]. The geometry of the polycrystal is then regularized by deleting small geometric entities (edges and arcs of ellipses) to prevent unreasonable mesh refinement. The microstructure obtained following the regularization process is illustrated in Fig. 1.

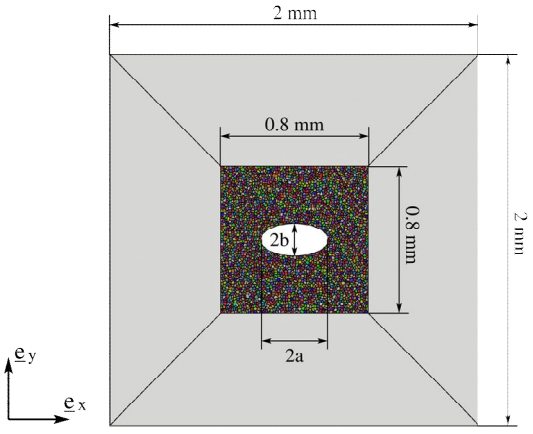

Figure 1. Shape and dimensions of the polycrystalline aggregate and the homogeneous matrix used in the finite element analysis.

In addition to the polycrystal, an elasto-plastic homogeneous matrix is modeled in order to avoid applying the boundary conditions directly on the edges of the microstructure. The polycrystal is subjected to three loading cycles in fully reversed uniaxial tension along the y-direction thanks to a homogeneous stress field applied on the upper and lower edges of the matrix.

The defect considered in this study is an elliptical hole characterized by its length $2a$ in the x-direction and its length $2b$ in the y-direction. Three defect sizes $2a$ (95 µm, 365 µm and 510 µm) and three ratios b/a (0.5, 1.0 and 1.5) are studied.

The orientation of the crystal coordinate system of each grain, with respect to the reference frame of the polycrystal, is characterized by three angles called Euler angles. Ten orientation sets, made up of 3265 triplets of Euler angles selected to be representative of the texture of the material tested [3], are used. Consequently, the response of 10 different realizations of microstructure is investigated per defect size.

The mesh generator Gmsh [5] is used to discretize the geometries with three-node triangular elements. Each grain is discretized in average with 14 elements and a generalized plane strain hypothesis is adopted.

Constitutive model of the single crystal

Due to the face-centered cubic lattice of the austenitic crystals, the elastic behavior is described by a linear cubic elasticity model characterized by three material parameters C_{1111}, C_{1122} and C_{1212} defined in the crystal coordinate system. The values of these parameters, calibrated for a Fe–18Cr–14Ni steel by Teklu et al. [6], are given in Table 1. The constitutive model used to describe the single crystal viscoplastic behavior of the crystals comes from the work of Méric et al. [7]. In this model, the plastic slip, which occurs along the close-packed lattice planes $\{111\}$ in the close-packed directions $\left[\bar{1}10\right]$, is described for each slip system s with the following flow rule:

$$\dot{\gamma}_s = \left\langle \frac{\left|\tau_s - \chi_s\right| - r_0 - r_s}{K} \right\rangle_+^n \operatorname{sgn}\left(\tau_s - \chi_s\right) = \dot{v}_s \operatorname{sgn}\left(\tau_s - \chi_s\right) \tag{1}$$

where τ_s is the resolved shear stress acting on the slip system s, r_0 is the initial critical shear stress, χ_s and r_s are respectively the kinematic and isotropic hardening variables associated to the slip system s, K and n are the parameters controlling the viscosity. The resolved shear stress τ_s acting on the slip system s, characterized by a unit vector normal to the slip plane $\underline{n}_s$ and a unit vector collinear to the slip direction $\underline{l}_s$, can be computed from the stress tensor $\underline{\underline{\sigma}}$ as follows:

$$\tau_s = \left(\frac{\underline{n}_s \otimes \underline{l}_s + \underline{l}_s \otimes \underline{n}_s}{2} \right) : \underline{\underline{\sigma}} \tag{2}$$

Non-linear hardening rules are used to describe the isotropic hardening variable r_s and the kinematic hardening variable χ_s:

$$r_s = Q \sum_r h_{sr} \left(1 - e^{-b v_r}\right) \tag{3}$$

$$\dot{\chi}_s = c\,\dot{\gamma}_s - d\,\dot{v}_s\,\chi_s \tag{4}$$

The material parameters of the single crystal viscoplaticity model have been calibrated from low-cycle fatigue tests conducted in several loading conditions: tension, torsion and combined out-of-phase tension and torsion [4]. These parameters are summarized in Table 1.

Table 1. Material parameters of the single crystal constitutive model for a 316L steel

Cubic elasticity			Viscosity		Kinematic hardening	
C_{1111} (GPa)	C_{1122} (GPa)	C_{1212} (GPa)	K (MPa.s$^{1/n}$)	n	c (MPa)	d
198	125	122	10	10	$2.04\cdot10^5$	$3.63\cdot10^3$

Isotropic hardening								
r_0 (MPa)	Q (MPa)	b	h_0	h_1	h_2	h_3	h_4	h_5
87.0	1.06	4.88	1	1	0.438	77.2	4.31	2.41

Constitutive model of the homogeneous matrix

The elastic behavior of the homogeneous matrix is described by a linear isotropic elasticity model characterized by the Young's modulus E and the Poisson's ratio ν. The rate-independent plasticity model is defined by a von Mises yield function:

$$f = \sqrt{\frac{3}{2}\left(\underline{\underline{\sigma}}^d - \underline{\underline{X}}^d\right) : \left(\underline{\underline{\sigma}}^d - \underline{\underline{X}}^d\right)} - \sigma^y - R \tag{5}$$

with σ^y, $\underline{\underline{\sigma}}$, $\underline{\underline{X}}$ and R corresponding respectively to the initial yield stress, the stress tensor, the backstress tensor and the isotropic hardening variable. The superscript $\bullet^d$ indicates the deviatoric part of a given tensor. The non-linear functions describing the rates of the isotropic hardening variable R and of the backstress tensor are defined by Eqs 6 and 7.

$$\dot{R} = B\left(Q_\infty - R\right)\dot{p} \tag{6}$$

$$\dot{\underline{\underline{X}}} = \frac{2}{3} C\,\dot{\underline{\underline{\varepsilon}}}^p - \gamma\,\underline{\underline{X}}\,\dot{p} \tag{7}$$

In Eqs 6 and 7, p and $\underline{\underline{\varepsilon}}^p$ denotes respectively the equivalent plastic strain and the plastic strain tensor and Q_∞, B, C and γ are material parameters. The set of

parameters of this elasto-plastic constitutive model have been calibrated for a 316L steel [4] and are given in Table 2.

Table 2. Material parameters of the macroscopic constitutive model for a 316L steel

Isotropic elasticity		Yield stress	Isotropic hardening		Kinematic hardening	
E (GPa)	ν	σ^y (MPa)	Q_∞ (MPa)	B	C (MPa)	γ
194	0.284	129	142	6.88	$7.05 \cdot 10^5$	$3.08 \cdot 10^3$

FATIGUE CRITERIA

Definition of the fatigue criteria

The determination of the fatigue strength requires specific fatigue criteria to accurately estimate the detrimental effect of a small notch. In order to address this issue, two multiaxial fatigue criteria, previously discussed, are considered in the present work:
- a probabilistic fatigue criterion based on a distribution of the crack initiation threshold,
- a deterministic criterion relying on a fatigue damage process zone.

Three mechanical quantities, computed from the mesoscopic stress tensors (i.e. the stress tensor averaged per grain) obtained during the last loading cycle of the FEA, are used in the definition of these fatigue criteria: the amplitude of the shear stress $\tau_a(\underline{n})$, the amplitude of the normal stress $\sigma_{n,a}(\underline{n})$ and the mean normal stress $\sigma_{n,m}(\underline{n})$, each acting on the slip plane of unit normal vector $\underline{n}$ (see Ref. [3] for the definitions of these quantities).

Probabilistic fatigue criterion

The probabilistic criterion, presented in [3], is based on the hypothesis that a fatigue crack initiates on the slip plane of unit normal vector $\underline{n}$ if the amplitude of the shear stress $\tau_a(\underline{n})$ acting on this plane exceeds a threshold $\tau_a^{th}(\underline{n})$. Assuming that this threshold is a Weibull distributed random variable, the probability $P_{Fn}(\underline{n})$ that a fatigue crack initiation occurs on the slip plane is:

$$P_{Fn}(\underline{n}) = P\left(\tau_a(\underline{n}) \geq \tau_a^{th}(\underline{n})\right) = 1 - \exp\left[-\left(\frac{\tau_a(\underline{n})}{\tau_0(\underline{n})}\right)^m\right] \tag{8}$$

where $\tau_0(\underline{n})$ and m are respectively the scale and the shape parameters of the Weibull distribution. In order to account for the effect of the normal stress on the fatigue strength, the scale parameter $\tau_0(\underline{n})$ depends on the mean and the alternating part of the normal stress (respectively $\sigma_{n,m}$ and $\sigma_{n,a}$) as follows:

$$\tau_0(\underline{n}) = \tau_0' \frac{1 - b\,\sigma_{n,m}(\underline{n})}{1 + a\left(\sigma_{n,a}(\underline{n}) / \tau_a(\underline{n})\right)} \tag{9}$$

The failure probability of a grain P_{Fg} is then assumed to correspond to the maximum value, among the set of four slip planes Δ, of the failure probability $P_{Fn}(\underline{n})$:

$$P_{Fg} = \max_{\underline{n}\in\Delta}\left[P_{Fn}(\underline{n})\right] \tag{10}$$

The weakest-link hypothesis, which means that the polycrystal fails when the weakest grain fails, is used in order to define the failure probability of a polycrystal P_{Fa} containing N_g grains:

$$1 - P_{Fa} = \prod_{g=1}^{Ng}\left(1 - P_{Fg}\right) \tag{11}$$

Deterministic fatigue criterion

The deterministic criterion discussed in this section has been presented in a previous study [4]. Summarily, this criterion relies on the assumption that the fatigue crack initiation occurs if an equivalent stress σ_{eq} averaged over a given grain set G_{PZ} exceeds a threshold γ:

$$\sigma_{eq,w} = \sum_{g\in G_{PZ}}\left[f_g\,\sigma_{eq}\right] \geq \gamma \tag{12}$$

with f_g corresponding to the volume fraction of the grain g. The equivalent stress σ_{eq} is defined for each grain as the maximum value, among the set of four slip planes Δ, of a linear combination of $\tau_a(\underline{n})$, $\sigma_{n,a}(\underline{n})$ and $\sigma_{n,m}(\underline{n})$:

$$\sigma_{eq} = \max_{\underline{n}\in\Delta}\left[\tau_a(\underline{n}) + \alpha\,\sigma_{n,a}(\underline{n}) + \beta\,\sigma_{n,m}(\underline{n})\right] \tag{13}$$

The grain set G_{PZ}, which can be seen as a fatigue damage process zone, is build in two steps. First, the grain with the highest value of equivalent stress σ_{eq}, is determined. This critical grain constitutes the first element of the set G_{PZ}. Then, the grains included in the first N_n neighborhoods are added to the set G_{PZ}. A grain g is considered in the neighborhood n if at least one of its nodes is on the boundary of one of the grains in the neighborhood $n-1$.

Calibration and predictions of the fatigue criteria

The calibration of four parameters is required for each criterion:

- a and α which describe the detrimental effect of $\sigma_{n,a}(\underline{n})$ on the fatigue strength,
- b and β which characterize the sensitivity of the fatigue limit to $\sigma_{n,m}(\underline{n})$,
- τ_0' and γ which are related to the fatigue limit in terms of $\tau_a(\underline{n})$,
- m and N_n which allow to weight the effect of a notch on the fatigue strength.

The results from the FEA of microstructures loaded at the average fatigue limit level, in different loading conditions, are required to calibrate these parameters. The loading conditions, applied on the unnotched polycrystal and selected to obtain various distributions of the local stress states, are the fully reversed uniaxial tension, the fully reversed shear and the uniaxial tension with a loading ratio $R = 0.1$. In the case of the probabilistic (resp. deterministic) criterion, the parameters m (resp. N_n) is imposed and the remaining parameters are calibrated such that the failure probability of the polycrystal P_{Fa} (resp. the weighted equivalent stress $\sigma_{eq,w}$) is, in average on the 10 different realizations of microstructures, equal to 0.5 (resp. γ) for each of the three loading conditions. The values of m and N_n are chosen so that the fatigue limits predicted in fully reversed uniaxial tension, in the case where $b/a = 1.0$ and for the three defect sizes $2a$, are as much as possible in accordance with those determined experimentally.

The fatigue criteria are then used to predict the average fatigue limits for the other geometries of elliptical hole studied. For a given ratio b/a and defect size $2a$, the average fatigue limit is predicted by determining the macroscopic stress amplitudes $\Sigma_{yy,a}$ which have to be applied to the matrix such as, in average on the 10 realizations:

- P_{Fa} is equal to 50% in the case of the probabilistic criterion,
- $\sigma_{eq,w}$ is equal to γ in the case of the deterministic criterion.

The predictions obtained for each criterion are presented, along with the experimental data, in a diagram "$\Sigma_{yy,a}$-$2a$" (see Fig. 2). It can be observed that both criteria satisfactorily predict the detrimental effect of a circular hole on the fatigue limit in fully reversed tension. Indeed, the maximum differences observed do not exceed 6% in the case of the probabilistic criterion and 10% in the case of the deterministic criterion. Moreover, the ellipse aspect ratio b/a does not affect significantly the predictions of the fatigue criteria, at least for the considered ranges of defect sizes $2a$ and ratio b/a, especially in the case of the probabilistic criterion where the difference does not exceed 5%. Nevertheless, it appears that an increase in the aspect ratio b/a, i.e. an increase in the radius of curvature $\rho = b^2/a$ in the critical regions of the ellipse, leads to a decrease of the average fatigue limit. These results are in accordance with the experimental trends observed by Billaudeau et al. [2] in the case of notches with stress concentration factors ranging from 2 to 4.

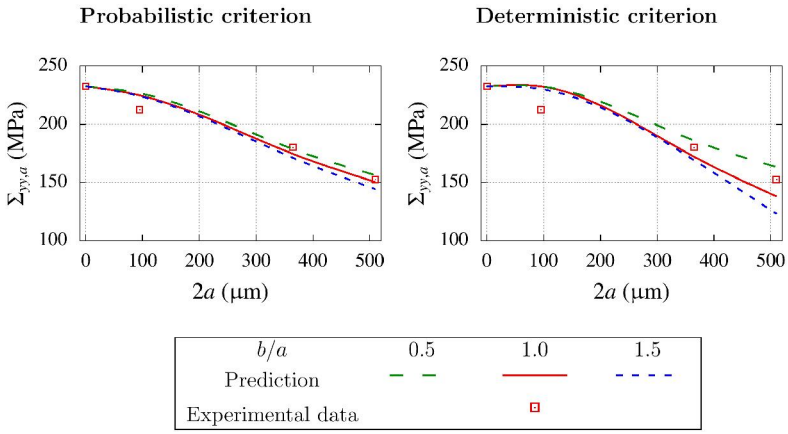

Figure 2. Fatigue limits determined experimentally and predicted by the criteria as a function of defect size $2a$ for different ellipse aspect ratio b/a .

CONCLUSIONS

The mechanical state at the grain scale, in polycrystals containing a elliptical hole and loaded in fully reversed tension, has been obtained thanks to FEA. The predictions provided by two multiaxial fatigue criteria have been compared to the experimental fatigue limits in the case of a circular hole. A good agreement has been generally observed for the considered defect sizes. Moreover, both criteria predict that a decrease in the aspect ratio of the ellipse b/a leads to a slight increase in the average fatigue limit in fully reversed tension. These predictions are consistent with the experimental trends discussed by Billaudeau et al. in the case of a low-carbon steel, for the range of stress concentration factor studied.

REFERENCES

1. Murakami, Y., Endo, M. (1983) *Eng. Fract. Mech.* **17**, 1-15.
2. Billaudeau, T., Nadot, Y., Bezine, G. (2004) *Acta Mater.* **52**, 3911-3920.
3. Guerchais, R., Morel, F., Saintier, N., Robert, C. (2015) *Fatigue Fract. Eng. Mater. Struct.* **38**, 1087-1104.
4. Guerchais, R., Scalet, G., Constantinescu, A., Auricchio, F. (2016) *Int. J. Fatigue* **87**, 405-417.
5. Geuzaine, C., Remacle, J.-F. (2009) *Int. J. Numer. Methods Eng.* **79**, 1309-1331.
6. Teklu, A., Ledbetter, H., Kim, S., Boatner, L., McGuire, M., Keppens, V. (2004) *Metall. Mater. Trans. A* **35**, 3149-3154.
7. Méric, L., Cailletaud, G., Gaspérini, M. (1994) *Acta Metall. Mater.* **42**, 921-935.